

UCSF

UC San Francisco Previously Published Works

Title

Clinical translation of hyperpolarized <sup>13</sup>C pyruvate and urea MRI for simultaneous metabolic and perfusion imaging

Permalink

<https://escholarship.org/uc/item/5s68f47b>

Journal

Magnetic Resonance in Medicine, 87(1)

ISSN

0740-3194

Authors

Qin, Hecong

Tang, Shuyu

Riselli, Andrew M

et al.

Publication Date









2022

DOI

10.1002/mrm.28965

Peer reviewed

# Clinical translation of hyperpolarized $^{13}\text{C}$ pyruvate and urea MRI for simultaneous metabolic and perfusion imaging

Hecong Qin<sup>1,2</sup>  | Shuyu Tang<sup>1</sup>  | Andrew M. Riselli<sup>1</sup>  | Robert A. Bok<sup>1</sup> | Romelyn Delos Santos<sup>1</sup> | Mark van Criekinge<sup>1</sup> | Jeremy W. Gordon<sup>1</sup>  | Rahul Aggarwal<sup>3</sup> | Rui Chen<sup>4</sup> | Gregory Goddard<sup>5</sup> | Chunxin Tracy Zhang<sup>5</sup> | Albert Chen<sup>4</sup> | Galen Reed<sup>4</sup> | Daniel M. Ruscitto<sup>4</sup> | James Slater<sup>1</sup> | Renuka Sriram<sup>1</sup>  | Peder E. Z. Larson<sup>1,2</sup>  | Daniel B. Vigneron<sup>1,2</sup>  | John Kurhanewicz<sup>1,2</sup> 

<sup>1</sup>Department of Radiology and Biomedical Imaging, University of California, San Francisco, San Francisco, California, USA

<sup>2</sup>Graduate Program in Bioengineering, University of California, Berkeley and San Francisco, San Francisco, California, USA

<sup>3</sup>Department of Medicine, University of California, San Francisco, San Francisco, California, USA

<sup>4</sup>General Electric Healthcare, Milwaukee, Wisconsin, USA

<sup>5</sup>General Electric Research, Niskayuna, New York, USA

## Correspondence

John Kurhanewicz, Professor of Radiology and Biomedical Imaging, Pharmaceutical Chemistry, and Urology, University of California, San Francisco (UCSF), 1700 4th St., Suite 203, Box 2520, San Francisco, CA 94143, USA.

Email: John.Kurhanewicz@ucsf.edu

## Present address

Shuyu Tang, HeartVista Inc., Los Altos, California, USA

## Funding information

National Institute of Health, Grant/Award Number: P41EB013598 and R01CA214554

**Purpose:** The combined hyperpolarized (HP)  $^{13}\text{C}$  pyruvate and urea MRI has provided a simultaneous assessment of glycolytic metabolism and tissue perfusion for improved cancer diagnosis and therapeutic evaluation in preclinical studies. This work aims to translate this dual-probe HP imaging technique to clinical research.

**Methods:** A co-polarization system was developed where  $[1-^{13}\text{C}]$ pyruvic acid (PA) and  $[^{13}\text{C}, ^{15}\text{N}_2]$ urea in water solution were homogeneously mixed and polarized on a 5T SPINlab system. Physical and chemical characterizations and toxicology studies of the combined probe were performed. Simultaneous metabolic and perfusion imaging was performed on a 3T clinical MR scanner by alternatively applying a multi-slice 2D spiral sequence for  $[1-^{13}\text{C}]$ pyruvate and its downstream metabolites and a 3D balanced steady-state free precession (bSSFP) sequence for  $[^{13}\text{C}, ^{15}\text{N}_2]$ urea.

**Results:** The combined PA/urea probe has a glass-formation ability similar to neat PA and can generate nearly 40% liquid-state  $^{13}\text{C}$  polarization for both pyruvate and urea in 3-4 h. A standard operating procedure for routine on-site production was developed and validated to produce 40 mL injection product of approximately 150 mM pyruvate and 35 mM urea. The toxicology study demonstrated the safety profile of the combined probe. Dynamic metabolite-specific imaging of  $[1-^{13}\text{C}]$ pyruvate,  $[1-^{13}\text{C}]$ lactate,  $[1-^{13}\text{C}]$ alanine, and  $[^{13}\text{C}, ^{15}\text{N}_2]$ urea was achieved with adequate

This is an open access article under the terms of the Creative Commons Attribution-NonCommercial-NoDerivs License, which permits use and distribution in any medium, provided the original work is properly cited, the use is non-commercial and no modifications or adaptations are made.

© 2021 The Authors. *Magnetic Resonance in Medicine* published by Wiley Periodicals LLC on behalf of International Society for Magnetic Resonance in Medicine.

spatial (2.6 mm × 2.6 mm) and temporal resolution (4.2 s), and urea images showed reduced off-resonance artifacts due to the  $J_{\text{CN}}$  coupling.

**Conclusion:** The reported technical development and translational studies will lead to the first-in-human dual-agent HP MRI study and mark the clinical translation of the first HP  $^{13}\text{C}$  MRI probe after pyruvate.

#### KEYWORDS

clinical translation, hyperpolarization, metabolism, perfusion, pyruvate, urea

## 1 | INTRODUCTION

With cancer therapeutic advancements contributing to a decrease in cancer mortality rate,<sup>1</sup> new diagnostic tools are needed to guide treatment selection and disease management. In vivo tumor biology assessment afforded by molecular imaging is essential for tumor phenotype characterization, treatment selection, and early evaluation of therapeutic response or resistance. Metabolism and perfusion are desirable imaging targets as altered cellular metabolism and tissue perfusion are mechanistically involved in cancer pathophysiology.<sup>2-4</sup> Combined metabolic and perfusion imaging techniques, such as [ $^{15}\text{O}$ ]water and [ $^{18}\text{F}$ ]fluorodeoxyglucose (FDG) positron emission tomography (PET), have been used clinically to identify aggressive breast,<sup>5</sup> lung,<sup>6</sup> and cervical<sup>7</sup> tumors and to evaluate tumor response to therapy.<sup>8,9</sup> However, multi-probe PET scans require multiple imaging sessions as the scanner cannot differentiate signals from multiple radiopharmaceuticals. In contrast, hyperpolarized (HP)  $^{13}\text{C}$  MR has the unique capability of simultaneous multi-probe imaging: MR spectroscopic imaging can distinguish the signal of  $^{13}\text{C}$ -labeled metabolic products by their unique chemical shifts, allowing real-time assessment of multiple metabolic fluxes and physiologic processes. For instance,  $^{13}\text{C}$ -labeled pyruvate and urea can be co-polarized and co-administered in a single imaging session,<sup>10</sup> and have been used extensively in preclinical studies.<sup>11-17</sup> Two HP  $^{13}\text{C}$  pyruvate isotopomers, [1- $^{13}\text{C}$ ]pyruvate and [2- $^{13}\text{C}$ ]pyruvate, are currently used in clinical trials to image tumor metabolism for improved diagnosis and therapeutic evaluation,<sup>18,19</sup> setting the stage for the clinical translation of other HP  $^{13}\text{C}$  imaging probes.

In this work, we aim to translate a dual-probe HP imaging technique using [1- $^{13}\text{C}$ ]pyruvate and [ $^{13}\text{C}$ ,  $^{15}\text{N}_2$ ]urea for simultaneous metabolic and perfusion imaging (Figure 1A). Pyruvate is a critical intermediate in cellular energy metabolism, positioned at the intersection of several metabolic pathways. The conversion rates from pyruvate to lactate, alanine,  $\text{CO}_2$ /bicarbonate, and other Krebs's cycle intermediates reflect the expression and activity of relevant transporters and enzymes. Unlike HP  $^{13}\text{C}$  pyruvate, HP  $^{13}\text{C}$  urea is a metabolically inactive, extracellular probe;

its MR signal is not affected by metabolic conversions but reflects blood flow, tissue perfusion, and volume of distribution.<sup>11,13,16,20</sup> The synergy between HP  $^{13}\text{C}$  pyruvate and urea MR is evident, as metabolism and perfusion often have opposite changes in disease progression and therapeutic response, such as enhanced metabolism but defective perfusion in high-grade compared to low-grade tumors,<sup>8,13,15,21</sup> and decreased metabolism but increased perfusion in therapeutic responders compared to non-responders.<sup>16,22</sup> The combined HP  $^{13}\text{C}$  pyruvate and urea MR could also evaluate tumor hypoxia, a critical biological modulator of cancer progression and treatment response.<sup>13,21,23</sup> Moreover, HP  $^{13}\text{C}$  urea could potentially improve the analysis of HP  $^{13}\text{C}$  pyruvate metabolism kinetics by providing independent assessments on bolus arrival and vascular input. Additionally, [ $^{13}\text{C}$ ,  $^{15}\text{N}_2$ ]urea has the advantage of longer  $T_1$  at low field (mitigating polarization loss during sample transfer) and long  $T_2$  (allowing higher in vivo signal)<sup>24</sup> compared to [ $^{13}\text{C}$ ]urea. Taken together, the preclinical evidence provided a strong rationale for the clinical investigation of simultaneous metabolic and perfusion MR with HP [1- $^{13}\text{C}$ ]pyruvate and [ $^{13}\text{C}$ ,  $^{15}\text{N}_2$ ]urea.

Herein, we report the technical development and translational studies toward dual-probe HP MR human imaging. First, we developed a co-polarization system for  $^{13}\text{C}$  pyruvate and urea compatible with the clinical polarizer. We then systematically characterized the probe performance, identified and quantified the impurities in the injection product, and developed standard operating procedures (SOP) for routine on-site production of sterile co-polarized probes. Finally, we performed toxicology and preclinical imaging feasibility studies for clinical translation.

## 2 | METHODS

### 2.1 | Co-polarization system for clinical studies

In preclinical studies,  $^{13}\text{C}$  urea powder is dissolved in an excipient such as glycerol to generate high probe

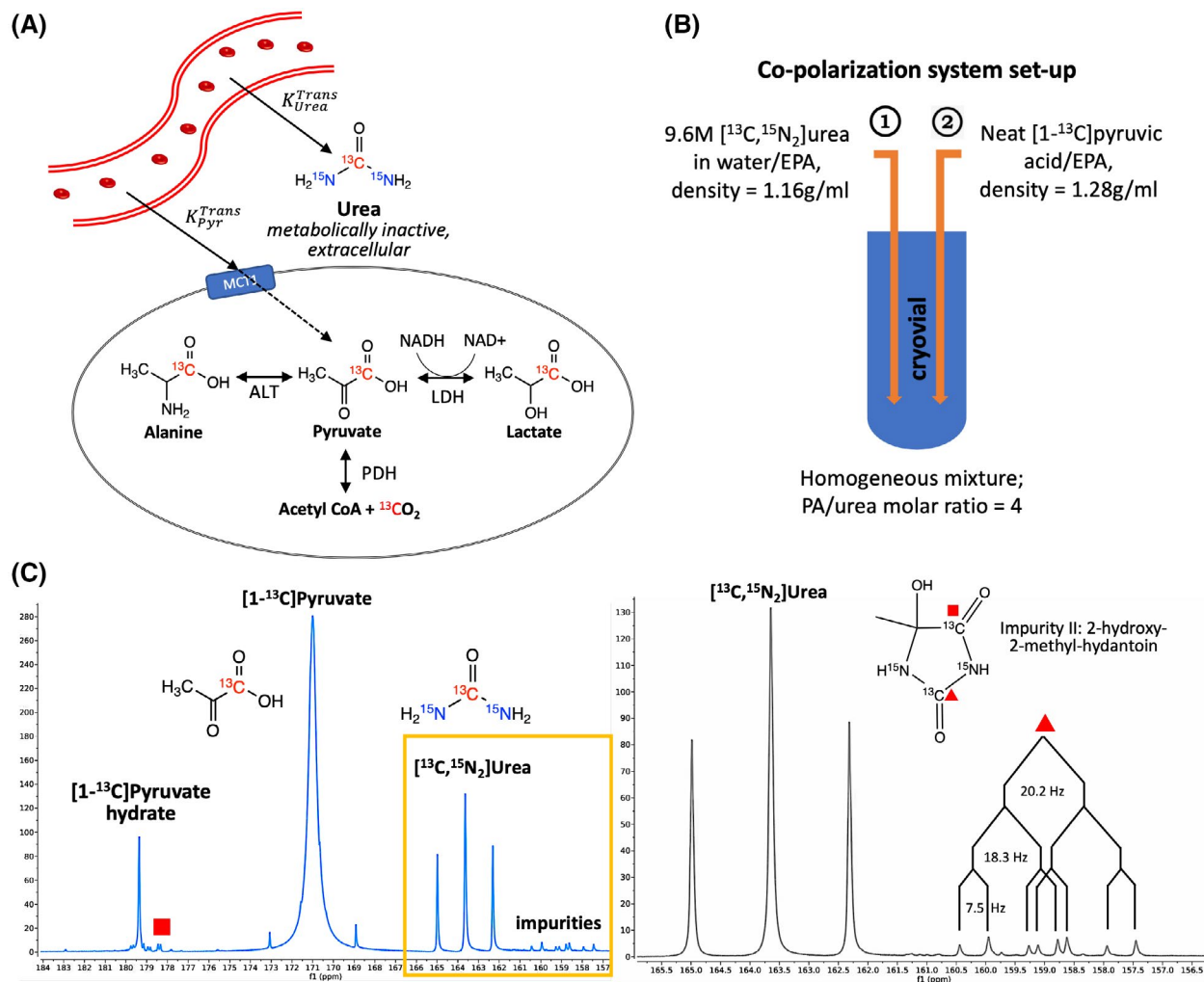


**FIGURE 1** A, Imaging mechanism: hyperpolarized  $[^{13}\text{C}]$ pyruvate and urea are intravenously administered in a single bolus, then leave the vasculature and enter the extracellular space (indicated by the solid line). Pyruvate can enter the cell at a slower rate compared to the vascular delivery (indicated by the dashed line) and be metabolized into lactate, alanine, or  $\text{CO}_2$ /bicarbonate, evaluating multiple metabolic fluxes. In contrast, urea is predominately extracellular and metabolically inactive, serving as a perfusion sensing probe. ( $K^{\text{trans}}$ , vascular transfer constant; MCT, monocarboxylate transporter; LDH, lactate dehydrogenase; ALT, alanine transaminase; PDH, pyruvate dehydrogenase). B, Co-polarization system set up: urea/water/EPA mixture (lower density) is loaded into cryovial first, then PA/EPA mixture is added (higher density), resulting in a homogeneous mixture of PA and urea with a molar ratio of 4:1 (PA, pyruvic acid; EPA, electron paramagnetic agent). C, Representative  $^{13}\text{C}$  NMR spectra of hyperpolarized  $[1-^{13}\text{C}]$ pyruvate and  $[^{13}\text{C},^{15}\text{N}_2]$ urea. The right spectrum zooms in the boxed region of the left spectrum, showing urea and Impurity II with relevant coupling constants ( $J_{\text{CN}} = 20.2$  Hz,  $J_{\text{CN}} = 18.3$  Hz,  $J_{\text{CC}} = 7.5$  Hz)

concentration (about 6 M) and provide glass-forming ability, which ensures the proximity between  $^{13}\text{C}$  nuclei and electrons at dynamic nuclear polarization (DNP) conditions. Next, neat pyruvic acid (PA) and urea/glycerol solution, each mixed with an electron paramagnetic agent (EPA), such as the trityl radical (AH111501 sodium), are sequentially frozen in the cryovial with minimal or no contact with each other.<sup>10</sup> This approach requires delicate manual manipulation of the cryovial and loading samples in frozen state into the polarizer, making it unsuitable for routine on-site production for clinical use. Additionally, glass-forming excipients are often exogenous compounds with high osmolality, which are undesirable for human injection.

Based on these considerations, the co-polarization system was re-designed to eliminate glass-forming excipients and sequential freezing of the cryovial (Figure 1B). To prepare the imaging probes for DNP,  $[^{13}\text{C},^{15}\text{N}_2]$ urea (GMP grade; ISOTEC, MilliporeSigma, Miamisburg, OH) was first dissolved in water (approximately 1:1 weight ratio) to generate a 9.6 M urea solution, then mixed with AH111501 (12.5 mM) before being loaded into the cryovial. Next, neat  $[1-^{13}\text{C}]$ PA (GMP grade; ISOTEC, MilliporeSigma, Miamisburg, OH) and a AH111501 (12.5 mM) mixture was loaded on top of urea solution. PA can penetrate the urea layer due to its higher density (1.28 g/mL) than urea solution (1.16 g/mL), resulting in a homogeneous mixture consisting of approximately 10 M

[1- $^{13}\text{C}$ ]PA, 2.5 M [ $^{13}\text{C}$ ,  $^{15}\text{N}_2$ ]urea, and 12.5 mM AH111501 in the cryovial.

## 2.2 | Differential scanning calorimetry

Differential scanning calorimetry (DSC; TA instrument, New Castle, DE) was used to characterize glass-formation ability of the imaging probe mixture. Neat PA and PA/urea mixture with a wide range of PA/urea concentration ratios (from 9.4:1 to 0.96:1) were studied, with a cycling temperature of  $-90$  to  $40$  °C. Detailed experimental parameters are reported in Supporting Information Section I (available online).

## 2.3 | Hyperpolarization

Approximately 1.1 mL combined  $^{13}\text{C}$  PA and urea probe was polarized on a 5T SPINlab system (GE Healthcare, Waukesha, WI) operating at 0.8 K. The sample was polarized with 139.97 GHz microwave irradiation for 3–4 h, then rapidly dissolved in 41 mL super-heated ( $130$  °C), pressurized sterile water and subsequently neutralized using equivalent sodium hydroxide (NaOH) and Tris(hydroxyethyl)aminomethane (Tris).

## 2.4 | Colorimetric quantification of urea concentration

Samples with unknown urea concentration were mixed at a 1:1 v/v ratio with a dye solution consisting of 1.2 M p-toluenesulfonic acid and 10 mM 4-(dimethylamino)cinnamaldehyde (DMAC) in a cuvette of 1 cm in length. Absorbance at 527 nm wavelength was measured using a spectrophotometer (DH-2000-BAL, Ocean Insights, Orlando, FL), and the urea concentration was derived by comparing the measured absorbance to a calibration curve previously acquired using the same experimental set up.

## 2.5 | Nuclear magnetic resonance (NMR) spectroscopy

Hyperpolarized  $^{13}\text{C}$  NMR spectroscopy was acquired on a 1.41T bench-top NMR system (Oxford Instruments, UK) with the following parameters:  $5^\circ$  flip angle, 8000 Hz spectral width, 0.125 Hz spectral resolution, 8.7 s temporal resolution for total 50 repetitions. After the HP acquisition, the thermal equilibrium NMR signal was quantified with the following experimental parameters: 10% v/v  $\text{D}_2\text{O}$  for locking the magnet, 1% v/v Gd-DTPA (Magnevist<sup>®</sup>, Bayer, Whippany, NJ) and 20 s relaxation delay to fully relax  $^{13}\text{C}$  spins,  $90^\circ$  flip angle, and 1000 averages). Longitudinal relaxation ( $T_1$ )

time constants for [1- $^{13}\text{C}$ ]pyruvate and [ $^{13}\text{C}$ ,  $^{15}\text{N}_2$ ]urea were estimated from dynamic HP signal after corrections for radiofrequency (RF) depletions of the HP signal. Liquid-state polarization of the HP probe was estimated by comparing the first HP spectrum's signal to the thermal-equilibrium spectrum, then back-calculated to the time of dissolution using  $T_1$  time constants measured at 1.41T for each experiment (about 80 s for pyruvate and 50 s for urea).  $^{13}\text{C}$  NMR spectroscopy of starting material and manual dissolution product was acquired at an 11.7T system (Bruker Avance III) to corroborate with HP NMR studies. Detailed NMR methods are reported in Supporting Information Section III.

## 2.6 | Liquid chromatography-mass spectrometry (LC-MS)

Impurities in the co-polarized probes were analyzed using high-performance liquid chromatography (HPLC) coupled with quadrupole time-of-flight mass spectrometry (Q-TOF-MS) (Supporting Information Figure S14). Two- $\mu\text{L}$  of each sample was sent for analysis immediately after dissolution. A negative ionization mode was used. Impurity quantification ( $\mu\text{g}/\text{mL}$ ) was obtained by spiking the sample with an internal reference standard (Impurity II) and referencing a calibration curve (Supporting Information Figure S15). Detailed NMR methods are reported in Supporting Information Section IV.

## 2.7 | Toxicology study

Four groups of male Sprague Dawley rats (2–3 mo old, 0.40–0.55 kg body weight) were intravenously injected with 2.5 mL over 10 s of the following solution: (I) saline control,  $n = 3$ ; (II) HP co-polarized injection product (approximately 150 mM pyruvate, 35 mM urea),  $n = 10$ ; (III) impurity II (5-hydroxy-5-methyl-hydantoin; 40 mM in saline), 100-fold dose escalation,  $n = 5$ ; (IV) impurity III (5-methyl-5-ureido-hydantoin; 20 mM in saline),  $n = 5$ . Given that the human injection dose used in HP pyruvate clinical studies is 0.43 mL/kg body weight, Group II (HP co-polarized group) received a greater than 10 times dose escalation, and Group III and IV (impurity groups) received a greater than 100 times dose escalation. Animals' vital signs, including heart rate, respiratory rate, and oxygen saturation, were recorded before, during, and 20 min after the intravenous injection using a pulse oximeter (MouseOx<sup>®</sup>; Starr Life Sciences Corp, Oakmont, PA). The animals were monitored for clinical signs of toxicity for 2 wk after the injection and their body weights were recorded during the monitoring period. Blood samples were collected before, 20 min, and 2 wk after the injection for complete blood count (CBC) and

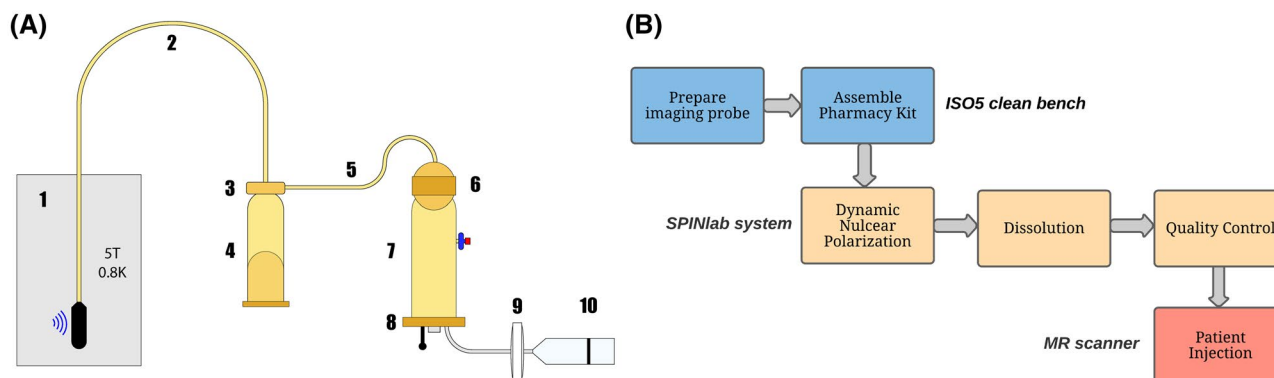


**FIGURE 2** A, Pharmacy Kit (fluid path) components: (1) cryovial in the SPINlab system with microwave irradiation; (2) dual-lumen dissolution tubing; (3) dissolution syringe valve; (4) dissolution syringe; (5) single-lumen transfer tubing; (6) electron paramagnetic agent (EPA) filter; (7) receiver vessel; (8) quality control (QC) plate with optical cuvette and NMR bulb; (9) sterility filter; (10) MedRad® syringe for patient administration. B, Co-polarized probe production process flowchart

liver-kidney function tests. The animals were sacrificed 2 wk after injection for gross pathological examination.

## 2.8 | In vivo hyperpolarized $^{13}\text{C}$ MRI

All animal experiments were performed according to the University of California, San Francisco Institutional Animal Care and Use Committee (IACUC) approved protocols. Adult Sprague Dawley rats ( $n = 3$ ) were imaged following HP co-polarized injection on a 3T clinical MR scanner (Discovery<sup>TM</sup> MR750; GE Healthcare, Milwaukee, WI). Adult rats were intravenously injected with 2.5 mL co-polarized [ $^{13}\text{C}$ ]pyruvate and [ $^{13}\text{C}$ ,  $^{15}\text{N}_2$ ]urea produced using the SOP described above. Dynamic MR images of pyruvate, alanine, lactate, and urea were acquired with volumetric coverage of the rat's body. Pyruvate, lactate, and alanine images were acquired using a metabolite-selective spiral gradient echo (GRE) sequence as previously reported,<sup>25</sup> with the following design parameters: 80 Hz RF pulse passband, 25.17 ms pulse length, 22 ms readout duration, and 88 ms repetition time (TR). Urea images were acquired using a balanced steady state free precession (bSSFP) sequence, with a non-spatially selective RF pulse with a 40 Hz passband and stopband, a 6 ms pulse length, and a 12.26 ms TR. The 3D stack-of-spiral readouts consist of 6 spiral readouts interleaved per phase encoding step for 16 phase-encoding steps (slices), with a 4 ms readout duration in each step to mitigate off-resonance effects. The following acquisition parameters were used: flip angles of lactate, alanine, pyruvate, and urea were  $30^\circ$ ,  $30^\circ$ ,  $8^\circ$ ,  $50^\circ$ ;  $2.6 \times 2.6 \times 21$  mm spatial resolution; 4.2 s temporal resolution.  $^{13}\text{C}$  dynamic MR acquisitions were automatically triggered after bolus arrival in the kidneys, using an autonomous scanning protocol, including real-time frequency and  $B_1$  field calibration, implemented on the RTHawk platform (HeartVista, Los Altos, CA) as previously described.<sup>26</sup>

## 3 | RESULTS

### 3.1 | Imaging probe characterization

Since stable glass formation is critical for DNP, we sought to characterize the glass-forming ability of the combined PA/urea probe using DSC. We found that PA/urea/water mixtures with 4:1 PA/urea ratio can form a stable glass with glass transition temperatures ( $T_g$ ) around  $-70$  to  $-80^\circ\text{C}$ . No crystallizations during the thaw-freeze cycle were observed (Supporting Information Figures S1 and S2). The combined PA/urea probe exhibited similar glass transition behaviors to neat PA, the most used HP imaging probe (Supporting Information Figures S3 and S4).

We then characterized the polarization performance of the combined PA/urea probe on a 5T SPINlab system. The combined PA/urea probe had a solid-state build-up constant of  $6340 \pm 1934$  s ( $n = 20$ ). After 3.5–4 h of 139.87 GHz microwave irradiation, the co-polarization system produced liquid state polarization of  $40.0 \pm 5.9\%$  for pyruvate,  $39.1 \pm 7.3\%$  for urea ( $n = 21$ ). A representative  $^{13}\text{C}$  NMR spectrum of HP injection product acquired on a 1.41T bench-top spectrometer is shown in Figure 1C.

### 3.2 | Standard operating procedure (SOP) development

We developed and optimized an SOP for routine on-site production of sterile co-polarized probes using the hardware and material that are currently used in HP  $^{13}\text{C}$  pyruvate clinical studies following with Good Manufacturing Practice (GMP) outlined in the U.S. Code of Federal Regulation Title 21, Part 212. Briefly, after [ $^{13}\text{C}$ ]PA and [ $^{13}\text{C}$ ,  $^{15}\text{N}_2$ ]urea are combined in the cryovial, a purpose-built, disposable fluid path (Pharmacy Kit, GE Healthcare, Milwaukee, WI) for dissolution is assembled (Figure 2A). The cryovial that contains

combined PA/urea (referred to as “starting material”) is then loaded into a SPINlab polarizer. After 3.5–4 h of microwave irradiation, the starting material is dissolved by superheated and pressurized sterile water for injection (SWFI) in the dissolution syringe (Part A) by a computer-controlled process. The part A dissolution then passes through a size-exclusion filter that traps EPA, which precipitates in the presence of pyruvic acid. Next, the dissolution product is neutralized by NaOH and Tris in the receiver vessel (Part B), producing HP media at physiologic temperature and pH (referred to as “injection product”). Finally, the co-polarized injection product passes through a terminal sterility filter before reaching the administering syringe. The materials used in the co-polarized probe formulation and fluid path assembly are reported in Table 1 and a flowchart of the production process is shown in Figure 2B. Neutralization media used in the receiver vessel (Part B) is designed to neutralize a wide range of pyruvic acid concentrations resulting from the varying amount of combined PA/urea probe recovered from the cryovial. A bench-top titration experiment was performed to validate the pH buffer capacity of the neutralization media, which demonstrated the buffer system could neutralize 125–190 mM pyruvic acid (Supporting Information Figure S5). The SOP was further validated by four consecutive successful Process Qualification trials (Supporting Information Table S1), which reproducibly generated over 40 mL of injection product consisting of approximately 150 mM sodium [ $^{13}\text{C}$ ]pyruvate and 35 mM [ $^{13}\text{C}$ ,  $^{15}\text{N}_2$ ]urea with physiologic temperature and pH.

### 3.3 | Quality control (QC) procedures

Immediately after dissolution, pyruvate concentration, residual EPA concentration, pH, temperature, and volume of HP co-polarized injection product were measured by the SPINlab QC system in an automated process. Acceptable ranges are listed in Supporting Information Table S2. The concentration of urea was indirectly estimated from pyruvate concentration based on the molar ratio of PA to urea in the formulation. We

also developed a colorimetric method to quantify urea concentration (Supporting Information Figure S6) and found the indirect estimations agreed with post-dissolution quantifications. To ensure the injection product’s sterility, the integrity of the terminal sterility filter was manually tested before releasing the injection product for administration. Endotoxin tests were also performed post-administration.

### 3.4 | Impurity investigation

Multiple low-intensity peaks neighboring pyruvate and urea peaks were observed on the  $^{13}\text{C}$  NMR spectrum of co-polarized [ $1\text{-}^{13}\text{C}$ ]PA and [ $^{13}\text{C}$ ,  $^{15}\text{N}_2$ ]urea (Figure 1C) but were not observed for individually polarized  $^{13}\text{C}$  pyruvate or urea, suggesting that these impurities arose from the co-polarization process. To identify and quantify these impurities, three sets of  $^{13}\text{C}$  NMR experiments were performed at 11.7T on the following samples: (1) individual raw materials ([ $^{13}\text{C}$ ]urea, [ $^{13}\text{C}$ ,  $^{15}\text{N}_2$ ]urea, and [ $1\text{-}^{13}\text{C}$ ]PA) for baseline structure elucidation and peak assignment (Supporting Information Figure S7); (2) starting material for co-polarization (PA/urea mixture) for impurity identification and structure elucidation (Supporting Information Figures S8–S11); (3) neutralized [ $1\text{-}^{13}\text{C}$ ]pyruvate and [ $^{13}\text{C}$ ,  $^{15}\text{N}_2$ ]urea injection product for impurity quantification (Supporting Information Figures S12 and S13). Detailed NMR impurity analyses are reported in Supporting Information Section III. Three novel impurity (I, II, III) compounds were identified in the starting material and injection products based on their unique chemical shifts and  $J_{\text{CC}}$  and  $J_{\text{CN}}$  coupling constants (Supporting Information Table S3); their presence was also confirmed by liquid chromatography-mass spectrometry (LC-MS) (Supporting Information Figures S16 and S17). These impurities are likely to be the cross-reaction product of [ $1\text{-}^{13}\text{C}$ ]pyruvic acid and [ $^{13}\text{C}$ ,  $^{15}\text{N}_2$ ]urea during the fluid path assembly process (Figure 3). Impurity II (5-hydroxy-5-methyl-hydantoin) was found to be the most prominent novel impurity compound in the injection product ( $1.71 \pm 0.26\%$  molar concentration by LC-MS, and 2% by NMR), while the percent molar

**TABLE 1** Pharmacy kit (fluid path) composition for co-polarized [ $1\text{-}^{13}\text{C}$ ]pyruvate and [ $^{13}\text{C}$ ,  $^{15}\text{N}_2$ ]urea probes

Components	Chemical composition	Function
Cryovial	1.098 g ( $\pm 2\%$ ) neat [ $1\text{-}^{13}\text{C}$ ]pyruvic acid*	Metabolism-sensing probe
	0.378 g ( $\pm 2\%$ ) 9.6 M [ $^{13}\text{C}$ , $^{15}\text{N}_2$ ]urea in SWFI*	Perfusion-sensing probe
	*Mixed with 12.5 mM AH111501 sodium salt	Electron paramagnetic agent
Dissolution syringe (Part A)	41 g $\pm$ 0.05 g SWFI	Heated and pressurized to dissolve frozen imaging probe in the cryovial
Receiver vessel (Part B)	13.50 $\pm$ 0.05 g buffer solution (558 mM NaOH, 310 mM Tris, 351.4 mg/mL EDTA)	Neutralize pyruvic acid
	19.35 $\pm$ 0.05 g SWFI	Diluent

Abbreviations: EDTA, ethylenediaminetetraacetic acid; NaOH, sodium hydroxide; SWFI, sterile water for injection; Tris, Tris(hydroxyethyl)aminomethane.

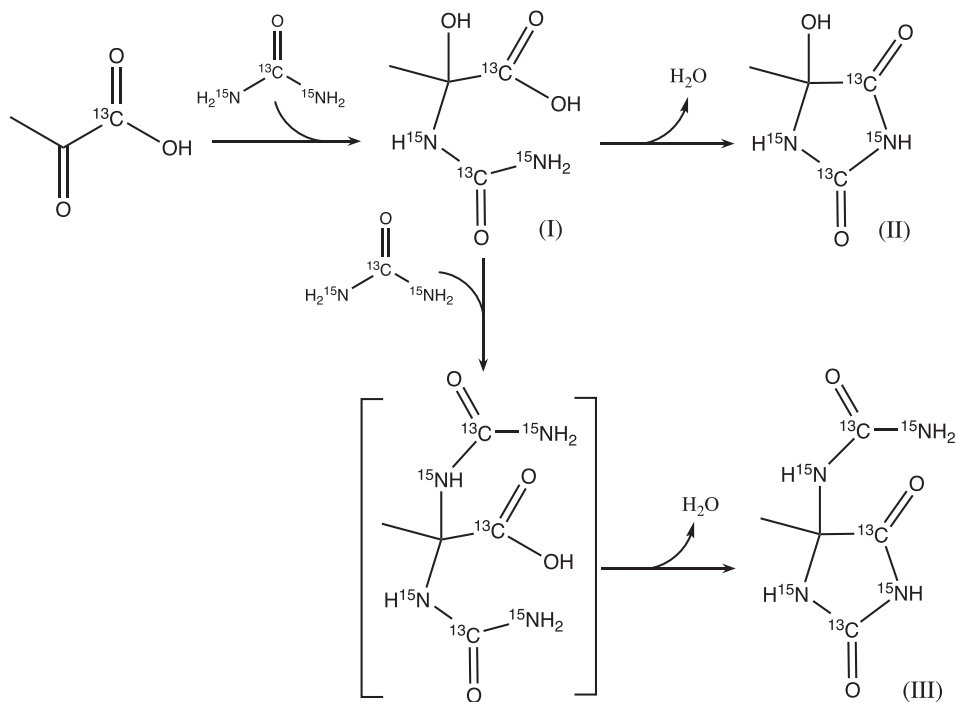


**FIGURE 3** Impurity formation scheme in co-polarized  $[1\text{-}^{13}\text{C}]$ pyruvate and  $[^{13}\text{C}, ^{15}\text{N}_2]$ urea. These reactions most likely occur in the cryovial at high-concentration conditions: the nucleophilic addition of urea (nitrogen) to pyruvic acid (C2 carbonyl carbon) yields Impurity I, an intermediate, which further undergoes intramolecular condensation between the carboxylate group and amide group, yielding Impurity II, a hydantoin. Impurity I can also undergo nucleophilic substitution with urea at C2 carbon before intramolecular condensation, yielding Impurity III, another hydantoin

concentration of Impurity I (2-hydroxy-2-ureido-propanoic acid) and Impurity III (5-methyl-5-ureido-hydantoin) were both estimated to be less than 0.5%. Based on the dose of 0.43 ml/kg used for HP  $^{13}\text{C}$  pyruvate studies,<sup>27</sup> the upper range of doses of Impurities II and III are 1.591  $\mu\text{mol}/\text{kg}$  and 0.39775  $\mu\text{mol}/\text{kg}$ , respectively, for an injection of 150 mM pyruvate and 35 mM urea. Further, only Impurity II was observed on HP  $^{13}\text{C}$  NMR spectra (Figure 1C), consistent with the finding that Impurity II is the predominant novel impurity in the dissolution product by NMR and LC-MS analyses.

### 3.5 | Toxicology study

We investigated the potential toxicities of the co-polarized injection products (the combination of pyruvate and urea) and the isolated novel impurity compounds (Impurity II and III). Four groups of Sprague Dawley rats were injected with normal saline ( $n = 3$ ), co-polarized injection product ( $n = 10$ ) with a 10-fold dose escalation, or isolated Impurity II or III ( $n = 5$  each) with a 100-fold dose escalation. All injections were well-tolerated and no significant physiological effects were observed either acutely or chronically for any group (Supporting Information Tables S4-S6). No significant changes in body weight or mortalities were observed during the 2-wk monitoring period after the injection for any

group (Supporting Information Table S7). Laboratory evaluations, including complete blood counts (CBC) (Supporting Information Table S8) and liver-kidney function tests (Supporting Information Table S9), showed no significant acute or chronic deviations from the saline control group, the group baselines, or reference ranges. No abnormalities of major organs were observed on gross pathological examination 2 wk after the injection. Finally, no behavioral abnormalities were observed in any of the animals studied.

### 3.6 | Imaging feasibility study

Although  $[^{13}\text{C}, ^{15}\text{N}_2]$ urea offers the advantage of reduced HP signal loss during sample transfer, the  $\text{AX}_2$  spin system of  $[^{13}\text{C}, ^{15}\text{N}_2]$ urea due to  $J$  coupling ( $J_{\text{CN}} = 20$  Hz, Figure 1C) can cause significant off-resonance artifacts when long readout trajectories are used. Moreover, the in vivo spectral region of the HP co-polarized study is crowded with  $[^{13}\text{C}]$  bicarbonate (163 ppm),  $[^{13}\text{C}, ^{15}\text{N}_2]$ urea (164 ppm),  $[1\text{-}^{13}\text{C}]$  pyruvate (171 ppm),  $[1\text{-}^{13}\text{C}]$ alanine (176 ppm),  $[1\text{-}^{13}\text{C}]$ pyruvate hydrate (181 ppm), and  $[1\text{-}^{13}\text{C}]$ lactate (183 ppm), making it challenging to perform dynamic, frequency-specific imaging with adequate spatial coverage and temporal resolution. In this study, we developed a 3D balanced steady-state free precession (bSSFP) sequence to image  $[^{13}\text{C}, ^{15}\text{N}_2]$



urea, consisting of urea frequency-selective RF excitation pulses (Figure 4A) and interleaved stack-of-spiral readouts.<sup>25</sup> This acquisition method was designed to use HP signal efficiently, minimize RF perturbations to other metabolites (Figure S18A), and mitigate off-resonance artifacts using repeated RF refocus pulses and a short readout duration (4 ms). Additionally, the 12.26 ms TR was designed to minimize spectral banding artifacts overlapping with other metabolites (Figure S18B). Pyruvate, lactate, and alanine were imaged using a multi-slice spiral GRE sequence as previously reported.<sup>25</sup> Simultaneous metabolic and perfusion imaging was achieved by alternatively applying a multi-slice 2D spiral GRE sequence for pyruvate and its metabolites and a 3D bSSFP sequence for urea.

Compared to single-shot spiral GRE images of urea, bSSFP images showed considerably reduced image blurring due to off-resonance artifacts, where the kidney cortex can be distinguished from the medulla (Figure 4B,C). In the images of sum metabolite signal of a kidney slice (Figure 4C), lactate signal predominates in the kidney, while pyruvate signal predominates the vasculature (aorta and vena cava) and gastrointestinal tracts are highlighted on alanine images. These findings are consistent with the imaging probe distribution and organ metabolism profiles. A plot of HP signal dynamics of pyruvate, lactate, alanine, and urea in the kidney and vasculature (aorta and vena cava) is shown in Figure 4D, where pyruvate and urea signals peak in about 5 s in the vasculature

and in about 10 s in the kidney after the start of acquisition (with 5 s acquisition delay from the start of injection), whereas lactate and alanine signal gradually build up during the acquisition window.

## 4 | DISCUSSION

The interplay between metabolism and perfusion is involved in tumorigenesis, disease progression, and resistance to therapy, making metabolism and perfusion desirable cancer imaging markers. However, combined metabolic and perfusion imaging often requires different imaging probes, acquisition techniques, or even modalities. HP  $^{13}\text{C}$  MR is a promising molecular imaging technique to non-invasively study in vivo physiologic processes, with the unique capability of simultaneous multi-probe imaging.<sup>10,28</sup> In this report, we present clinical translation efforts to incorporate a new perfusion-sensing probe, HP [ $^{13}\text{C}$ ,  $^{15}\text{N}_2$ ]urea, into the existing HP  $^{13}\text{C}$  pyruvate MR exams.

We first developed a co-polarization system for [ $^{13}\text{C}$ ]PA and [ $^{13}\text{C}$ ,  $^{15}\text{N}_2$ ]urea where PA provides glass-forming ability and eliminates the glass-forming excipient for urea. The short-range order in the glass, an amorphous state, ensures the uniform proximity of  $^{13}\text{C}$  nuclei and unpaired electrons in the EPA, a requirement for DNP. PA, urea, and water can form an extensive hydrogen bonding network, preventing crystallization by raising the energy barrier for molecular

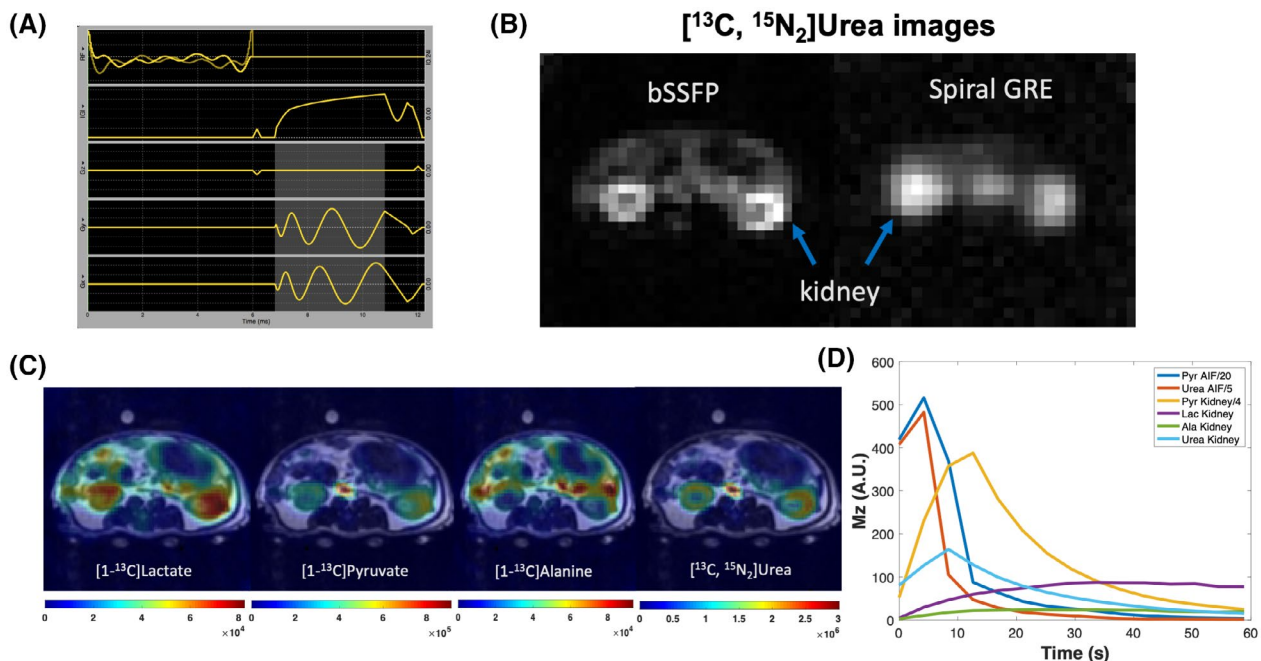


**FIGURE 4** A, A pulse sequence diagram of bSSFP sequence for HP  $^{13}\text{C}$  urea acquisition (highlighted area indicates readout duration). B, bSSFP sequence produced superior image quality (signal-to-noise ratio, resolution, sharpness) compared to the single-shot spiral GRE sequence. C, Representative simultaneously acquired metabolism and perfusion images of an adult rat: sum HP signals of each metabolite were overlaid on  $T_2$  weighted images; flip angles of lactate, alanine, pyruvate, and urea were  $30^\circ$ ,  $30^\circ$ ,  $8^\circ$ ,  $50^\circ$ , with  $2.5 \times 2.5 \times 21$  mm spatial resolution and 4.2 s temporal resolution. D, HP signal dynamics in the aorta and kidneys of an adult rat

reorganization and favoring glass formation.<sup>29-31</sup> Other attractive intermolecular forces such as dipole-dipole interactions among non-hydrogen bonding motifs in PA and urea also contribute to the glass forming ability.<sup>32</sup> Indeed, we observed that the combined PA/urea probe with a wide range of PA/urea ratios has a reliable glass-forming ability, with the glass transition temperature ( $T_g$ ) like neat PA. Moreover, because the physical stability of glass below  $T_g$  is related to glass-forming ability,<sup>33,34</sup> the fact that the polarizer temperature (0.8 K) is well-below the  $T_g$  of the combined PA/urea probe (~ 200 K) ensures the glass stability during DNP.

The 4 to 1 molar ratio of PA to urea in the formulation was chosen based on glass stability, target probe concentrations in the final injection product, and imaging feasibility. Quantification of metabolic fluxes requires sufficient in vivo SNR of downstream metabolic products of pyruvate.<sup>35</sup> Since the starting material amount is limited by the cryovial volume, pyruvate content was prioritized for higher in vivo SNRs of pyruvate, lactate, and alanine. Further, since urea is dissolved in water, a higher urea content increases the water content of the formulation, increasing the likelihood of localized crystallization while reducing the glass forming ability. This formulation can generate nearly 40% liquid-state  $^{13}\text{C}$  nuclear polarization for both pyruvate and urea in 3-4 h, comparable to the PA-alone formulation, and produce 40 mL of approximately 150 mM pyruvate and 35 mM urea in the final injection product. Although the final urea concentration is lower than previously reported in preclinical studies,<sup>13,14,16,36</sup> the  $^{15}\text{N}$  labeling renders [ $^{13}\text{C}$ ,  $^{15}\text{N}_2$ ]urea with longer  $T_1$  at low field (mitigating polarization loss during sample transfer) and longer  $T_2$  (higher in vivo signal) compared to [ $^{13}\text{C}$ ]urea, compensating for the lower concentration.

We developed an SOP for routine on-site production to reproducibly generate sterile HP [1- $^{13}\text{C}$ ]pyruvate and [ $^{13}\text{C}$ ,  $^{15}\text{N}_2$ ] urea injection products of acceptable probe concentration, pH, temperature, and volume with negligible residual EPA. There are several differences in the formulation and production processes for the combined PA/urea probe compared to PA-alone production. First, EPA concentration was reduced to 12.5 mM from 15 mM in PA-alone formulation because 15 mM EPA formulation was observed to have faster solid-state build-up but lower final polarization. The reduced EPA amount also facilitated its removal during the dissolution steps. Second, the amount of neutralization media in the Part B receiver vessel was also reduced due to the reduced amount of PA in the cryovial, which also resulted in a lower osmolality of the combined HP  $^{13}\text{C}$  pyruvate and urea injection compared to the HP  $^{13}\text{C}$  pyruvate injection. Third, the SWFI volume in the Part A dissolution syringe (superheated and pressurized component) was increased to 41 g from 37.45 g to accommodate the increased heat capacity of the combined PA/urea probe compared to neat PA, which improved the sample recovery rate from the cryovial.

Pyruvic acid and urea can undergo slow cross-reactions under high concentration conditions,<sup>37</sup> which motivated us to investigate impurities in the co-polarized probe. Using hyperpolarized NMR, high resolution thermal equilibrium NMR, and LC-MS techniques, three novel impurity products were identified and quantified. The  $^{13}\text{C}$  and  $^{15}\text{N}$  labeling of the probes facilitated the impurity identifications:  $J_{\text{CC}}$  and  $J_{\text{CN}}$  coupling patterns and constants are consistent with the chemical structures of impurities, in particular atom arrangement and bond lengths (Supporting Information Table S3).  $^{13}\text{C}$  and  $^{15}\text{N}$  labeled molecules have unique mass/charge ratio on LC-MS compared to their natural abundance counterparts, which confirmed the chemical structures identified by the NMR analysis. Moreover, the NMR and LC-MS techniques complemented each other's detection limit. Impurity I in the injection product was observed by NMR but not LC-MS, whereas Impurity III was observed by LC-MS but not NMR. Based on NMR and MS findings, Impurity II was found to be the predominant impurity (1-2%) while Impurities I and III exist at lower concentrations (<0.5%). The qualitative and quantitative information obtained from impurity investigation further guided design of the toxicology study.

Pyruvate and urea are endogenous molecules whose toxicity has been extensively studied. HP  $^{13}\text{C}$  pyruvate injection (consisting of pyruvate, Tris, ethylenediaminetetraacetic acid [EDTA], and trace amount of AH11501) is currently used in clinical research studies, and its toxicology profiles were previously reported in the HP pyruvate Phase I clinical trial.<sup>38</sup> Moreover, the toxicology of the known impurities in the HP  $^{13}\text{C}$  pyruvate injection, including AH112623 (parapyruvate), AH112615 (Tris-pyruvate), and AH113462 (lactone), has previously been studied. Intravenous urea has been administered clinically to treat glaucoma,<sup>39</sup> cerebral edema,<sup>40,41</sup> and hyponatremia<sup>42</sup> at a dose of 1-1.5 g/kg body weight, about a thousand-fold higher than the HP co-polarized injection dose (0.8-1.3 mg/kg body weight of urea). Moreover, the parenteral urea drug product Ureaphil (Hospira) 40 g/vial was previously approved by the U.S. Food and Drug Administration (FDA). Therefore, we focused this toxicology study on investigating the potential toxicities of the co-polarized injection product and the isolated novel impurity compounds, for which no prior safety data are available. Using injection products allows the characterization of biological effects of combined pyruvate and urea along with novel impurities. Two additional groups of rats were injected with Impurity II or III as isolated compounds to achieve further dose escalation. Impurity I was not studied as an isolated compound because of its negligible concentration and intermediate nature. No signs of toxicities associated with the combined pyruvate and urea probe were observed on any metrics studied, demonstrating its safety profile.

We further demonstrated the feasibility of simultaneously imaging [1- $^{13}\text{C}$ ]pyruvate, its downstream metabolites, and

[ $^{13}\text{C}$ ,  $^{15}\text{N}_2$ ]urea on a clinical MR scanner with adequate spatial coverage and temporal resolution. The  $\text{AX}_2$  spin system of [ $^{13}\text{C}$ ,  $^{15}\text{N}_2$ ]urea (1:2:1 peak ratio) modulates the urea signal, causing off-resonance artifacts. Moreover, 25 ms after the start of spin system dephasing, spins of two side peaks are completely out of phase with spins of the central peak, creating a null signal in k-space ( $J_{\text{CN}} 20 \text{ Hz} \times 25 \text{ ms} = 0.5$  cycles/180-degree). In previous studies, bSSFP sequences with repeated RF refocus pulses and short readout durations to mitigate  $J_{\text{CN}}$  dephasing have been used to image [ $^{13}\text{C}$ ,  $^{15}\text{N}_2$ ]urea.<sup>24,43,44</sup> However, in these studies neither [ $^{1-13}\text{C}$ ]pyruvate nor its downstream metabolites were present to interfere with urea imaging. Moreover, these studies used Cartesian readout trajectories with a long scan time, which is not feasible for 3D dynamic imaging. Based on these considerations, we developed a urea frequency-specific bSSFP sequence with a stack-of-spiral readout trajectory and a short readout duration (4 ms) to mitigate off-resonance artifacts and avoid null signals in k-space. Additionally, the bSSFP sequence offers a two- to three-fold signal-to-noise ratio (SNR) advantage compared to the spiral GRE sequence,<sup>25</sup> and can further take advantage of the long in vivo  $T_2$  (about 10 s) of [ $^{13}\text{C}$ ,  $^{15}\text{N}_2$ ]urea by its efficient use of transverse magnetizations.<sup>24</sup> Pyruvate, alanine, and lactate images were sequentially acquired with a single-band spectral-spatial RF excitation and a single-shot spiral readout. Two sequences, bSSFP for urea and GRE for pyruvate and its metabolic products, were alternately applied to achieve simultaneous metabolic and perfusion imaging using commercially available software.

Our imaging approach has several limitations. First, the urea bSSFP sequence requires stringent RF pulse sequence design. The TR needs to be chosen carefully to avoid spectral banding artifact overlapping with non-urea resonances. The bSSFP acquisition is also sensitive to  $B_0$  inhomogeneity, which could cause metabolite resonance frequency inadvertently overlapping with spectral banding artifacts. Moreover, the urea RF pulse is not spatially selective because the long spectral-spatial RF pulse length is not compatible with the short TR of bSSFP sequences. Furthermore, the frequency-selective RF pulse enforces a 3D acquisition, which is sensitive to flow effects. Second, the  $^{13}\text{C}$  urea RF pulse has a passband and stopband of 40 Hz, leading to signal contamination from  $^{13}\text{C}$  bicarbonate (80 Hz apart from urea at 3T). This urea bSSFP sequence might be acceptable for initial cancer imaging studies, where mitochondrial activities and bicarbonate signal are low, but needs to be further modified to image the brain, heart, and other organs where bicarbonate signals are not negligible. Third, although readout time is considerably reduced using stack-of-spiral readout trajectory, off-resonance imaging artifacts are not eliminated. Off resonance corrections can be applied at the image reconstruction stage to improve image quality and metabolic quantification accuracy.<sup>45</sup> Finally, using two imaging sequences in a single

imaging session could complicate data analysis. A multi-echo acquisition approach (Iterative Decomposition of Echoes of Asymmetrical Length, IDEAL) can use prior knowledge of chemical shifts and relative peak ratios of urea to simultaneously image all metabolites using one acquisition sequence.<sup>12</sup>

In summary, we performed technical development and translational studies that enabled the clinical investigation of the combined HP  $^{13}\text{C}$  pyruvate and urea MR. This study leverages the unique capability of HP  $^{13}\text{C}$  MR for multi-probe imaging to achieve a simultaneous assessment of glycolytic metabolism and perfusion, thereby providing a multimeric evaluation of tumor biology in a single imaging session. In a future clinical trial, the reported imaging technique will be used to image prostate cancer before surgery, with post-surgery imaging-biology correlation. Although the combined HP  $^{13}\text{C}$  pyruvate and urea MR has been applied extensively in pre-clinical studies, the acquisition parameters and data analysis framework need to be optimized for human studies, where the probe arrival timing (due to cardiovascular circulation rate), subject physiologic state (awake vs. anesthetized), and imaging volume are considerably different from animal studies.

This work marks the clinical translation of the first HP MR probe after  $^{13}\text{C}$  pyruvate. Non-invasive assessments of in vivo metabolism and physiology afforded by HP  $^{13}\text{C}$  MR could potentially facilitate initial diagnosis, treatment planning, and therapeutic evaluation for patients with cancer, providing a useful tool for precision medicine.

## ACKNOWLEDGMENTS

We thank Jasmine Hu, Evelyn Escobar, Dr. Yaewon Kim, and Dr. David Korenchan for their assistance with experiments and David Taylor for editorial assistance. We acknowledge funding support from the U.S. National Institute of Health (R01CA214554, P41EB013598). We also acknowledge the administrative and technical support provided by the Surbeck Lab of Advanced Imaging and the Biomedical NMR Lab at the University of California, San Francisco (UCSF). Additionally, HQ acknowledges Ph.D. fellowships from the UCSF Graduate Division.

## CONFLICT OF INTEREST









J.K., P.L., and D.V. received grants from the U.S. National Institute of Health along with General Electric during the conduction of this work and outside the submitted work. PL declares personal fees from Human Longevity, Inc, outside the submitted work. R.C., G.G., C.T.Z., A.C., G.R., and D.R. are employees of General Electric. ST is an employee of HeartVista Inc. Other authors have no conflicts of interest to declare.

## DATA AVAILABILITY STATEMENT

The authors declare that the data supporting the findings of this study are available within the paper and its Supporting

Information. Raw data are available from the corresponding author upon reasonable requests.

## ORCID

Hecong Qin  <https://orcid.org/0000-0003-2618-8366>  
 Shuyu Tang  <https://orcid.org/0000-0002-9911-482X>  
 Andrew M. Riselli  <https://orcid.org/0000-0002-0714-5726>  
 Jeremy W. Gordon  <https://orcid.org/0000-0003-2760-4886>  
 Renuka Sriram  <https://orcid.org/0000-0003-3505-2479>  
 Peder E. Z. Larson  <https://orcid.org/0000-0003-4183-3634>  
 Daniel B. Vigneron  <https://orcid.org/0000-0001-5795-8699>  
 John Kurhanewicz  <https://orcid.org/0000-0002-3544-5339>

## REFERENCES

- Howlader N, Forjaz G, Mooradian MJ, et al. The effect of advances in lung-cancer treatment on population mortality. *N Engl J Med*. 2020;383:640-649.
- Hanahan D, Weinberg RA. The hallmarks of cancer. *Cell*. 2000;100:57-70.
- Hanahan D, Weinberg RA. Hallmarks of cancer: the next generation. *Cell*. 2011;144:646-674.
- Welch DR, Hurst DR. Defining the hallmarks of metastasis. *Cancer Res*. 2019;79:3011-3027.
- Specht JM, Kurland BF, Montgomery SK, et al. Tumor metabolism and blood flow as assessed by positron emission tomography varies by tumor subtype in locally advanced breast cancer. *Clin Cancer Res*. 2010;16:2803-2810.
- van Elmpt W, Das M, Hüllner M, et al. Characterization of tumor heterogeneity using dynamic contrast enhanced CT and FDG-PET in non-small cell lung cancer. *Radiother Oncol*. 2013;109:65-70.
- Apostolova I, Hofheinz F, Buchert R, et al. Combined measurement of tumor perfusion and glucose metabolism for improved tumor characterization in advanced cervical carcinoma. A PET/CT pilot study using [15O]water and [18F]fluorodeoxyglucose. *Strahlenther Onkol*. 2014;190:575-581.
- Dunnwald LK, Gralow JR, Ellis GK, et al. Tumor metabolism and blood flow changes by positron emission tomography: relation to survival in patients treated with neoadjuvant chemotherapy for locally advanced breast cancer. *J Clin Oncol*. 2008;26:4449-4457.
- de Langen AJ, van den Boogaart V, Lubberink M, et al. Monitoring response to antiangiogenic therapy in non-small cell lung cancer using imaging markers derived from PET and dynamic contrast-enhanced MRI. *J Nucl Med*. 2011;52:48-55.
- Wilson DM, Keshari KR, Larson PEZ, et al. Multi-compound polarization by DNP allows simultaneous assessment of multiple enzymatic activities in vivo. *J Magn Reson*. 2010;205:141-147.
- von Morze C, Larson PEZ, Hu S, et al. Investigating tumor perfusion and metabolism using multiple hyperpolarized (13)C compounds: HP001, pyruvate and urea. *Magn Reson Imaging*. 2012;30:305-311.
- Lau AZ, Miller JJ, Robson MD, Tyler DJ. Simultaneous assessment of cardiac metabolism and perfusion using copolarized [1-13 C]pyruvate and 13 C-urea. *Magn Reson Med*. 2017;77:151-158.
- Chen H-Y, Larson PEZ, Bok RA, et al. Assessing prostate cancer aggressiveness with hyperpolarized dual-agent 3D dynamic imaging of metabolism and perfusion. *Cancer Res*. 2017;77:3207-3216.
- Lee JE, Diederich CJ, Bok R, et al. Assessing high-intensity focused ultrasound treatment of prostate cancer with hyperpolarized 13 C dual-agent imaging of metabolism and perfusion. *NMR Biomed*. 2018;32:e3962.
- Bok R, Lee J, Sriram R, et al. The role of lactate metabolism in prostate cancer progression and metastases revealed by dual-agent hyperpolarized 13C MRSI. *Cancers (Basel)*. 2019;11:257.
- Qin H, Zhang V, Bok RA, et al. Simultaneous metabolic and perfusion imaging using hyperpolarized 13C MRI can evaluate early and dose-dependent response to radiation therapy in a prostate cancer mouse model. *Int J Radiat Oncol Biol Phys*. 2020;107:887-896.
- Markovic S, Fages A, Roussel T, et al. Placental physiology monitored by hyperpolarized dynamic 13C magnetic resonance. *Proc Natl Acad Sci USA*. 2018;115:E2429-E2436.
- Kurhanewicz J, Vigneron DB, Ardenkjaer-Larsen JH, et al. Hyperpolarized 13C MRI: path to clinical translation in oncology. *Neoplasia*. 2019;21:1-16.
- Wang ZJ, Ohliger MA, Larson PEZ, et al. Hyperpolarized 13C MRI: state of the art and future directions. *Radiology*. 2019;291:273-284.
- von Morze C, Larson PEZ, Hu S, et al. Imaging of blood flow using hyperpolarized [(13)C]urea in preclinical cancer models. *J Magn Reson Imaging*. 2011;33:692-697.
- van Elmpt W, Zegers CML, Reymen B, et al. Multiparametric imaging of patient and tumour heterogeneity in non-small-cell lung cancer: quantification of tumour hypoxia, metabolism and perfusion. *Eur J Nucl Med Mol Imaging*. 2016;43:240-248.
- Mankoff DA, Dunnwald LK, Gralow JR, et al. Blood flow and metabolism in locally advanced breast cancer: relationship to response to therapy. *J Nucl Med*. 2002;43:500-509.
- Matsuo M, Matsumoto S, Mitchell JB, Krishna MC, Camphausen K. Magnetic resonance imaging of the tumor microenvironment in radiotherapy: perfusion, hypoxia, and metabolism. *Semin Radiat Oncol*. 2014;24:210-217.
- Reed GD, von Morze C, Bok R, et al. High resolution (13)C MRI with hyperpolarized urea: in vivo T(2) mapping and (15)N labeling effects. *IEEE Trans Med Imaging*. 2014;33:362-371.
- Tang S, Bok R, Qin H, et al. A metabolite-specific 3D stack-of-spiral bSSFP sequence for improved lactate imaging in hyperpolarized [1-13C]pyruvate studies on a 3T clinical scanner. *Magn Reson Med*. 2020;84:1113-1125.
- Tang S, Milshteyn E, Reed G, et al. A regional bolus tracking and real-time B1 calibration method for hyperpolarized 13 C MRI. *Magn Reson Med*. 2019;81:839-851.
- Tang S, Meng MV, Slater JB, et al. Metabolic imaging with hyperpolarized 13 C pyruvate magnetic resonance imaging in patients with renal tumors-Initial experience. *Cancer*. 2021;127:2693-2704.
- von Morze C, Bok RA, Reed GD, Ardenkjaer-Larsen JH, Kurhanewicz J, Vigneron DB. Simultaneous multiagent hyperpolarized (13)C perfusion imaging. *Magn Reson Med*. 2014;72:1599-1609.
- Wang R, Pellerin C, Lebel O. Role of hydrogen bonding in the formation of glasses by small molecules: a triazine case study. *J Mater Chem*. 2009;19:2747.
- Olgenblum GI, Sapir L, Harries D. Properties of aqueous trehalose mixtures: glass transition and hydrogen bonding. *J Chem Theory Comput*. 2020;16:1249-1262.
- Kaushal AM, Chakraborti AK, Bansal AK. FTIR studies on differential intermolecular association in crystalline and amorphous states of structurally related non-steroidal anti-inflammatory drugs. *Mol Pharm*. 2008;5:937-945.

32. Koperwas K, Adrjanowicz K, Wojnarowska Z, Jedrzejowska A, Knapik J, Paluch M. Glass-forming tendency of molecular liquids and the strength of the intermolecular attractions. *Sci Rep*. 2016;6:36934.
33. Alhalaweh A, Alzghoul A, Mahlin D, Bergström CAS. Physical stability of drugs after storage above and below the glass transition temperature: relationship to glass-forming ability. *Int J Pharm*. 2015;495:312-317.
34. Baird JA, Van Eerdenbrugh B, Taylor LS. A classification system to assess the crystallization tendency of organic molecules from undercooled melts. *J Pharm Sci*. 2010;99:3787-3806.
35. Larson PEZ, Chen H-Y, Gordon JW, et al. Investigation of analysis methods for hyperpolarized  $^{13}\text{C}$ -pyruvate metabolic MRI in prostate cancer patients. *NMR Biomed*. 2018;31:e3997.
36. Lau AZ, Miller JJ, Robson MD, Tyler DJ. Cardiac perfusion imaging using hyperpolarized ( $^{13}\text{C}$ ) urea using flow sensitizing gradients. *Magn Reson Med*. 2016;75:1474-1483.
37. Murahashi S, Yuki H, Kosai K, Doura F. Methylene-hydantoin and related compounds. I. On the reaction of pyruvic acid and urea: the synthesis of 5-methylene-hydantoin. *Bull Chem Soc Jpn*. 1966;39:1559-1562.
38. Nelson SJ, Kurhanewicz J, Vigneron DB, et al. Metabolic imaging of patients with prostate cancer using hyperpolarized [ $^{13}\text{C}$ ]pyruvate. *Sci Transl Med*. 2013;5:198ra108.
39. Keith CG. Intravenous urea in glaucoma. *Br J Ophthalmol*. 1961;45:307-311.
40. Javid M. Effect of urea on cerebrospinal fluid pressure in human subjects. *JAMA*. 1956;160:943.
41. Levin AB, Duff TA, Javid MJ. Treatment of increased intracranial pressure: a comparison of different hyperosmotic agents and the use of thiopental. *Neurosurgery*. 1979;5:570-575.
42. Reeder RF, Harbaugh RE. Administration of intravenous urea and normal saline for the treatment of hyponatremia in neurosurgical patients. *J Neurosurg*. 1989;70:201-206.
43. Nielsen PM, Szocska Hansen ES, Nørlinger TS, et al. Renal ischemia and reperfusion assessment with three-dimensional hyperpolarized  $^{13}\text{C}$ ,  $^{15}\text{N}_2$ -urea. *Magn Reson Med*. 2016;76:1524-1530.
44. Bertelsen LB, Nielsen PM, Qi H, et al. Diabetes induced renal urea transport alterations assessed with 3D hyperpolarized  $^{13}\text{C}$ ,  $^{15}\text{N}$ -urea. *Magn Reson Med*. 2017;77:1650-1655.
45. Man LC, Pauly JM, Macovski A. Improved automatic off-resonance correction without a field map in spiral imaging. *Magn Reson Med*. 1997;37:906-913.

## SUPPORTING INFORMATION

Additional Supporting Information may be found online in the Supporting Information section.

**FIGURE S1-S4** Differential Scanning Calorimetry (DSC) studies

**FIGURE S5** Validation of buffer capacity of neutralization media

**FIGURE S6** Urea concentration colorimetric quantification calibration curve

**FIGURE S7-S13** NMR impurity analysis

**FIGURE S14-S17** LC-MS analysis

**FIGURE S18** Urea-specific RF pulse designs

**TABLE S1** Process Qualification (PQ) trials to validate the standard operating procedure (SOP)

**TABLE S2** Quality Control (QC) tests for hyperpolarized [ $^{13}\text{C}$ ]pyruvate and [ $^{13}\text{C}$ ,  $^{15}\text{N}_2$ ]urea injection product

**TABLE S3** Structure and characterization of novel impurities

**TABLE S4-S7** Toxicology data

**How to cite this article:** Qin H, Tang S, Riselli AM, et al. Clinical translation of hyperpolarized  $^{13}\text{C}$  pyruvate and urea MRI for simultaneous metabolic and perfusion imaging. *Magn Reson Med*. 2022;87: 138–149. <https://doi.org/10.1002/mrm.28965>